Journal of
Materials Sciences and Applications

JScholar
Fostering Scholarly Communication

Research Article Open Access

Features of Crystalline and Magnetic Structure of Cobalt Ferrite Modified with Rare Earth Ions

BK Argymbek[1*], A Hashhash[2], DP Kozlenko[1], M Kaiser[2] and BN Savenko[1]

[1]Joint Institute for Nuclear Research, 141980, Dubna, Russia
[2]Reactor and Neutron Physics Department, Nuclear Research Center, Egyptian Atomic Energy Authority, Russia

***Corresponding authors:** BK Argymbek, Joint Institute for Nuclear Research, Dubna, Russia, Tel: +79256369044, E-mail: argymbek92@mail.ru

Received Date: April 06, 2021 **Accepted Date:** May 06, 2021 **Published Date:** May 08, 2021

Citation: BK Argymbek (2021) Features of Crystalline and Magnetic Structure of Cobalt Ferrite Modified with Rare Earth Ions. J Mater sci Appl 5: 1-11.

Abstract

The crystal and magnetic structure of spinel ferrite $CoFe_{2-x}Ce_xO_4$ with different Rare earth (RE) concentration ($x \leq 0.1$) were studied by means of X-ray diffraction (XRD), vibrating sample magnetometer (VSM) and neutron diffraction (ND). (XRD) confirms the formation of the samples in nano-scale with a single-phase cubic structure. The magnetic hysteresis *M-H* loops obtained from VSM at 100 K introduce magnetic parameters; M_s, H_c, M_r with values larger than their room temperature (RT) counterpart. The ND crystal parameters like as lattice parameters, interatomic bond lengths and the distribution of cations between octahedral and tetrahedral crystallographic positions as well as a magnetic moment of iron ions were obtained. With an increase in the concentration of cerium, a change in the corresponding bond lengths and the iron magnetic moment in the octahedral oxygen environment is observed due to the predominant occupation of this crystallographic position by cerium ions.

Keywords: XRD; VSM; Neutron Diffraction; Spinel Ferrites; Ferrimagnetism

Introduction

The spinel-type ferrite materials attract the attention of researchers due to their unique structural and magnetic properties [1]. Thus, due to the complex nature of redistribution of magnetic cations between different crystallographic positions in the spinel crystal structure these compounds show unusual types of magnetic ordering, the spine-glass states, incommensurate and canted magnetic structures [2-4]. Besides, those materials also have found different applications in industry and technologies [5-7] as transformer cores, radio frequency circuits, antennas, data storage devices, magnetic nanostructures, and etc.

The formation of unique magnetic properties in spinel ferrites is mainly due to redistribution of magnetic ions between two non-equivalent crystallographic positions in the face-centered cubic structure with the space group $Fd\ \bar{3}m$: crystallographic position A with tetragonal oxygen environment and position B with octahedral coordination one [8, 9]. It is accepted that all magnetic interactions in spinel ferrites are divided into three main groups: magnetic interactions between ions in position A (magnetic exchange interaction J_{AA}), magnetic interactions J_{BB} between cations in position B and exchange interactions between magnetic cations in different crystal positions – J_{AB} [9, 10]. It is believed that the magnetic interaction of J_{AB} is much stronger than the interactions of J_{AA} and J_{BB}, which leads to the stabilization of the ferrimagnetic state in mixed spinel types [10]. As, an example, for tetragonal ferrite, $ZnFe_2O_4$ is characterized by the filling of the iron ions in the octahedral positions only [11]. On the other hand, in the ferrite $MnFe_2O_4$, Fe^{3+} ions sits in both positions [12]. The changes in the doping ratio of Mn^{3+} and Zn^{3+} ions of the initial spinel compound leads to significant transformations in the magnetic properties of such compounds.

Another interesting ferrite is $CoFe_2O_4$ [13, 14]. In this ferrite compound, cobalt ions Co^{3+} fill both A and B crystallographic positions and the relative distribution could depend on the synthesis conditions or the size effect of granules [15] or nanoparticles [16]. The relative distribution of cobalt cations between different crystallographic positions, as well as the features of the magnetic structure of ferrite materials, can be successfully studied by means of the neutron diffraction method [15, 17, 18]. On the other hand, doping with non-magnetic ions with large ionic radius can be applied to targeted control the occupation of different cations in certain crystallographic positions [19]. Thus, such large ions mainly occupy the oxygen octahedra in cubic spinel structure, which leads to the redistribution of magnetic cations in the tetragonal crystallographic position [20] and as a result the changes in the magnetic structure of ferrites [21]. In our work, we had perform detailed studies of the crystal and magnetic structure of doped cobalt ferrites $CoFe_{2-x}Ce_xO_4$ for cerium concentration range 0-0.1 due to the further insight of structure-magnetic properties relationships in spinel ferrites.

Experimental techniques

The samples $CoCe_xFe_{2-x}O_4$, (x= 0.0, 0.03, 0.05, 0.1), prepared by chemical auto-combustion method [22]. The starting materials are the nitrates of Cobalt, Iron and Cerium. A stoichiometric ratio of citric acid with formula ($C_6H_6O_7$) used as an organic fuel to achieve the required temperature of reaction. The mixture of nitrates and fuel were dissolved in a small amounts of doubly distilled water, thereafter stirred for 2 h and heated to a temperature of (80 ^{0}C). The PH value of the solution is mandatory to be adjusted to 7–8 during the time of heating and stirring. By the end of the previous process the water evaporated, and a dry viscous gel is formed. Therefore, the burned gel converted to fluffy powder, which was collected and ground in an agate mortar to obtain a fine powder.

X-ray diffraction (XRD) performed by Rigaku diffractometer with Cu Kα-radiation (λ=1.5406 Å). (VSM) measurements obtained by using- Lake Shore Model 7410 (USA), at a temperature of 100 K and by Appling magnetic field up to 20 kOe. Neutron powder diffraction experiments at ambient conditions were performed with the DN-6 diffractometer [23] at the IBR-2 high-flux pulsed reactor (Frank Laboratory of Neutron Physics, Joint Institute for Nuclear Research, Dubna, Russia). Diffraction patterns were measured at a scattering angle of $2\theta = 90°$ with the resolution $\Delta d/d$=0.022 at d=2 Å. The typical exposure time of one neutron diffraction pattern was – 20 min. The analysis of neutron diffraction data was performed by the Rietveld method using the FullProf software package [24].

Results and discussion

X-ray diffraction

X-ray diffraction of the nano-ferrite samples $CoCe_xFe_{2-x}O_4$, (x= 0.0, 0.03, 0.05, 0.1) synthesized by chemical auto-combustion method shown in Figure 1. The results of XRD, published in our previous work [22], confirm the formation of the samples in nano-scale with a single phase cubic structure. The grain size (D) decreases with substitution ratio of Ce^{3+} in Co-ferrite system [22].

Low temperature (VSM) measurements

Magnetic hysteresis *M-H* loops obtained at 100 K by applying an external magnetic field of ±20 kG for $CoFe_{2-x}Ce_xO_4$, (x= 0.0, 0.03, 0.05, 0.1) samples are shown in Figure 2. The *M-H* results will be discussed based on: 1- the concentration of para-magnetic Ce^{3+} ions, which have no magnetization contributions in the spinel lattice [25-28]. 2- the ionic radius of cerium (1.03Å) is relatively larger than that of Fe^{3+} (0.64 Å). This indicates that Ce^{3+} substitutes Fe^{3+} only in octahedral B-site, which has radius larger than that of the tetrahedral A-site. Therefore, the magnetic moment of B-site gradually reduces by further addition of Ce^{3+}. Consequently, the net magnetic moment of the lattice decreases according to the equation: $M = [M_B - M_A]$, where M_A and M_B represents the magnetic moments of A and B sites, respectively [29-32]. These results confirmed with the neutron diffraction data obtained in section 3.3. Besides, the disparity in ionic radii between Ce^{3+} and Fe^{3+} can causes a disturbance in the structure by producing strain and disorder in the electronic state. For all the samples in the series $CoFe_{2-x}Ce_xO_4$, the hysteresis is clearly

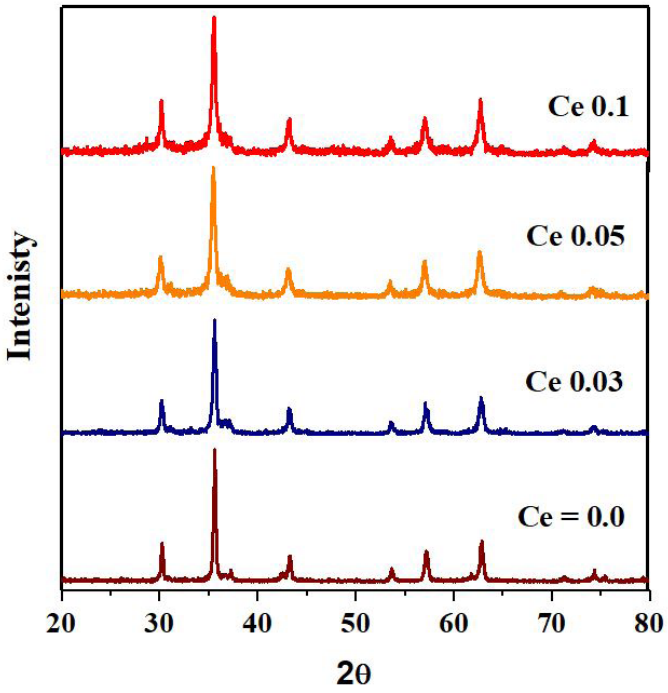

Figure 1: X-ray diffraction patterns of $CoFe_{2-x}Ce_xO_4$ measured at ambient conditions

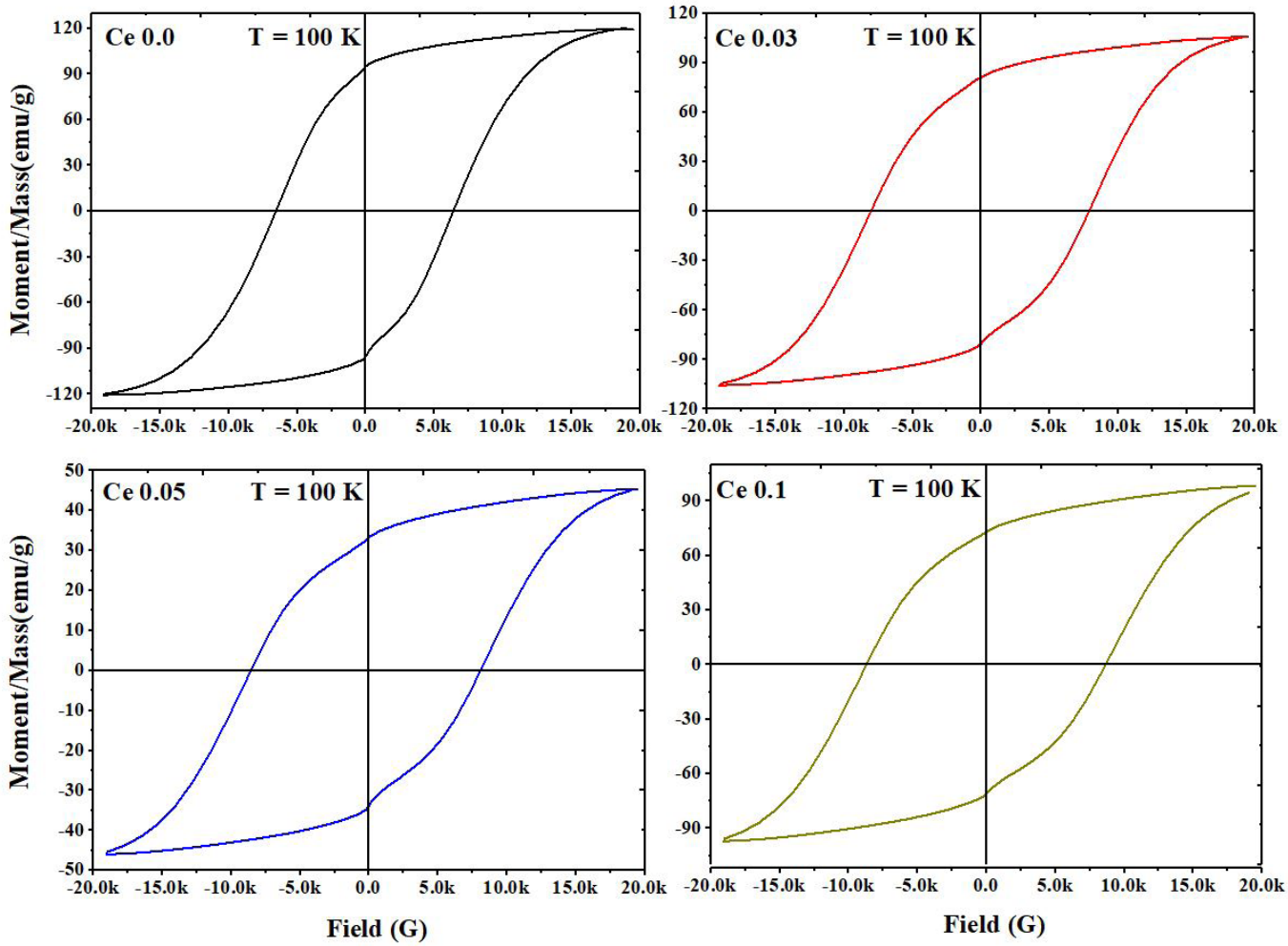

Figure 2: Magnetic hysteresis M-H loops obtained at 100 K by applying an external magnetic field of ±20 kG for $CoFe_{2-x}Ce_xO_4$

observed Figure 2. The magnetic parameters; M_s, H_c, M_r calculated from *M-H* loops at 100 K listed in Table 1, are found to be larger than their values estimated at room temperature (RT) [22]. One of the reasons for increasing such parameters at low temperature is that the magnetic moments are thermally fluctuated and reduced. The H_c values ranging between 6434 and 8682 G, while M_s and M_r values were 45.6-120 and 33.2-95.5 (emu/g) respectively. These values obtained at 100 K are indication of the ferrimagnetic nature (FM) of the Ce^{3+} substituted Co-ferrite [25]. Moreover, the substitution of RE in $CoFe_2O_4$ increases the degree of anisotropy and the spin orbit coupling in B-site. One the other hand, except for the sample with (x=0.1) the values of M_s decrease by further addition of Ce^{3+} Figure 3. Similar behavior obtained for the remanence values M_r Table 1. Pervious works reported that the magnetic parameters for nanoparticles can be changed due to the effect of grain size, strain and values of magnetic moments. The spin coupling interaction between magnetic ions through the 3d electrons is the main reason for the magnetic properties of ferrites. In case of rare earth addition the RE^{3+}-Fe^{3+} interaction happens by the 3d–4f coupling, which reduces the magnetic interaction through limitation of the charges exchange in the A- and B-sites. Moreover, the RE^{3+}–RE^{3+} interactions are negligible and consequently the magnetization are reduced [33, 34]. The squareness factor M_r/M_s, Table 1 with values > 0.5 confirms the existence of cubic magnetocrystalline anisotropy, which is an indication of the single domain structure [29, 35, 36]. When the major hysteresis loops is closed Figure 2, it is also another signature of the formation of a single domain, while all the irreversible hysteresis processes are completed [37].

Table 1: The deduced magnetic parameters for $CoCe_xFe_{2-x}O_4$ ($0.0 \leq x \leq 0.10$) samples obtained from the M-H loops at 100 K

Ce^{3+} content -x	M_s (emu/g)	H_c^+ (G)	H_c^- (G)	M_r (emu/g)	M_r/M_s
0.0	120	6434	-6515	95.5	0.791
0.03	105.5	7920	-7997	80.8	0.766
0.05	45.6	8139	-8529	33.2	0.737
0.1	97.7	8682	-8665	72.2	0.738

Neutron diffraction (ND)

The neutron diffraction patterns of the studied $CoFe_{2-x}Ce_xO_4$ ferrites with different cerium content are shown in Figure 4. All neutron patterns correspond to the cubic structure with the space group *Fd* $\bar{3}$*m [8]*. The obtained structural parameters of studied compounds are listed in Table 2. When cerium concentration increases, the lattice parameter of cubic structure grows (Figure 5a). The crystal structure of $CoFe_{2-x}Ce_xO_4$ ferrites contains oxygen octahedra with Fe/CoB-O and tetrahedral units with Fe/CoA-O (Figure 4b). The calculated from experimental data the bond lengths as a function of cerium concentration are shown in Figure 6.

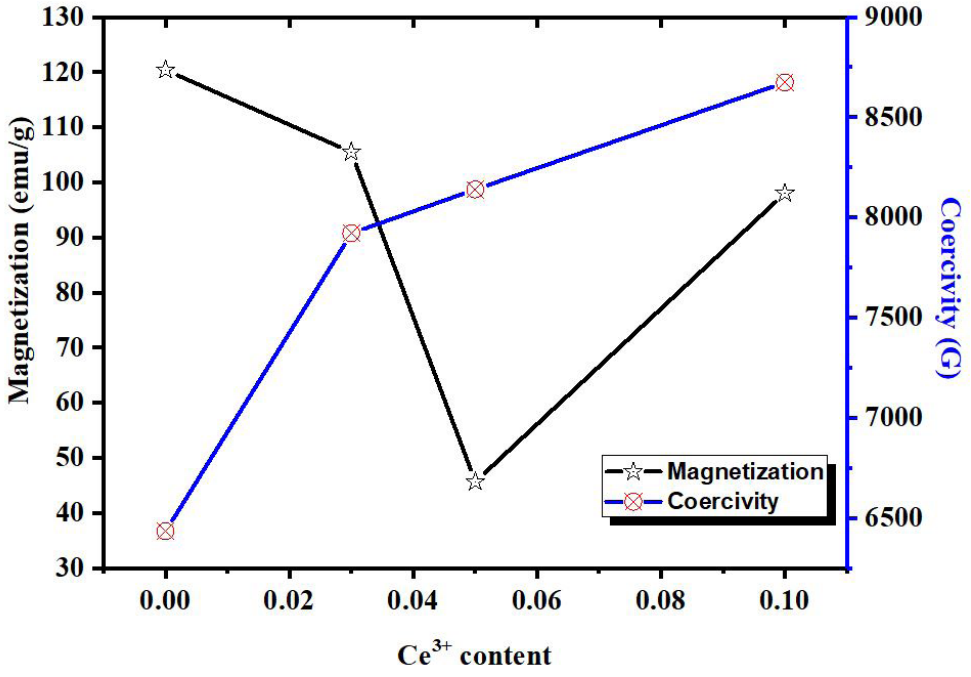

Figure 3: Dependences of the magnetization and coercivity on x for $CoFe_{2-x}Ce_xO_4$ ferrite

Table 2: The unit cell parameters, the Co/Fe-O bond length, the fractional coordinates of the oxygen atom, the average value of the magnetic moments of magnetic ions located in the positions A and B for the $CoFe_{2-x}Ce_xO_4$ compounds. In spinel crystal structure the Co and Fe cations distributed between crystallographic position B – 8(a) (1/8, 1/8, 1/8) and position A – 16(b) (1/2, 1/2, 1/2). The oxygen locates in positions 32(e) (x, x, x)

$CoFe_{2-x}Ce_xO_4$				
$(Co_{0.38}Fe_{0.62})[Co_{0.62}Fe_{1.33-x}Ce_x]O_4$				
Symmetry	$Fd\bar{3}m$			
x	0.1	0.05	0.03	0
Lattice parameters				
a (Å)	8.354(3)	8.353(3)	8.352(3)	8.350(3)
Bond-length				
Fe1-O1	1.989(3)	2.002(4)	1.801(4)	1.986(2)
Fe2-O1	2.005(3)	1.998(3)	2.182(3)	1.999(3)
Fe1-O2	1.932(4)	1.936(3)	1.939(3)	1.949(3)
Fe2-O2	2.027(3)	2.031(4)	2.035(3)	2.045(4)
Atomic coordinates				
O: x, y, z	0.256(2)	0.257(2)	0.256(3)	0.256(3)
Magnetic moment, M				
$((Fe1)^2+(Co1)^2)^{1/2}$ (μ_B)	3.56(3)	3.638(3)	3.790(3)	4.171(3)
$((Fe2)^2+(Co2)^2)^{1/2}$ (μ_B)	1.54(3)	1.619(3)	1.668(3)	1.799(3)

It is possible to calculate the distribution of cations between tetragonal and octahedral crystallographic positions from neutron diffraction data. The refined chemical compositions of studied ferrites including the distribution of the different crystallographic positions are listed in Table 2.

The concentration dependence of the bond lengths Fe/Co-O for octahedral and tetrahedral positions for ferrites $CoFe_{2-x}Ce_xO_4$ is shown in Figure 5b. We calculate the changes in the volumes of octahedral B and tetrahedral A crystallography units under variation of cerium content. The corresponding data is

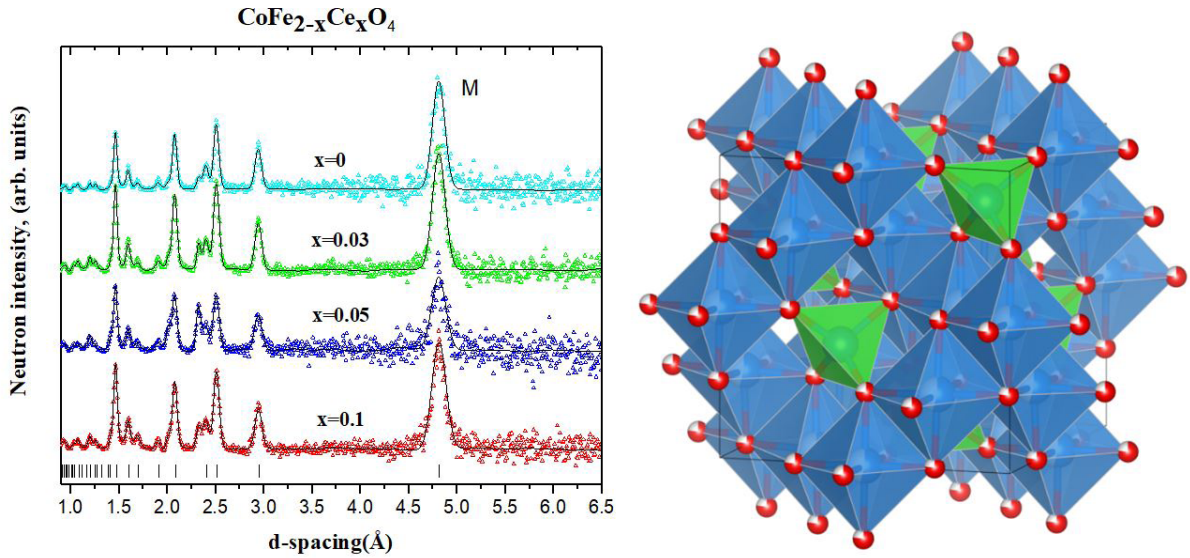

Figure 4: Neutron diffraction patterns of $CoFe_{2-x}Ce_xO_4$ measured at ambient conditions and refined by the Rietveld method. The experimental points and calculated profiles are shown. The ticks below represent the calculated positions of the structural peaks of cubic phase of studied ferrites. The magnetic reflections are labeled as «M». The cubic crystal structure of $CoFe_{2-x}Ce_xO_4$ compounds of Fd $\bar{3}$m symmetry. The octahedra units are labeled by blue, the tetragonal units are green

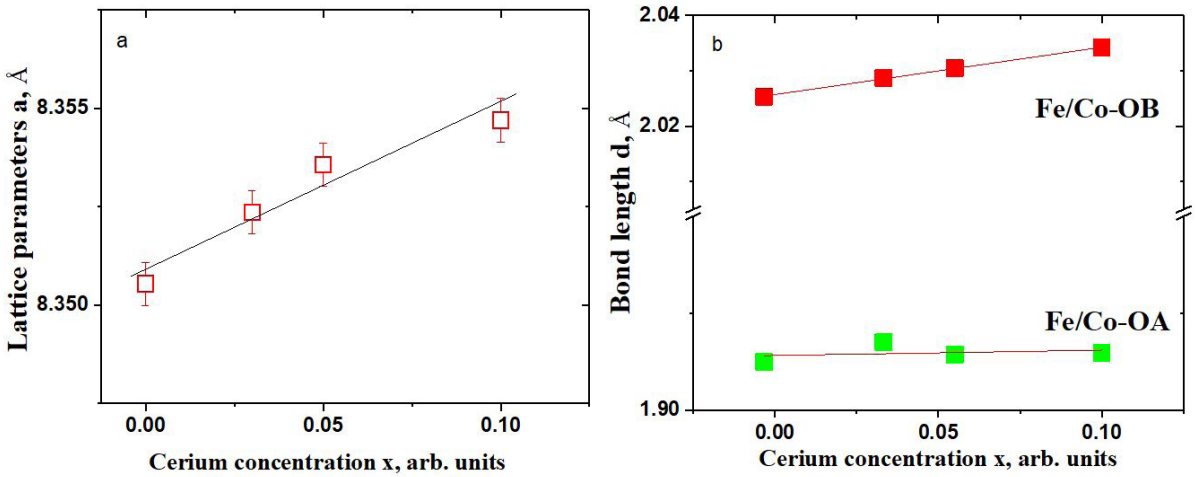

Figure 5: The lattice parameter of $CoFe_{2-x}Ce_xO_4$ ferrite as a function of cerium concentration. The solid line is linear approximation of experimental data. The Fe/Ce-O bond lengths of octahedral and tetrahedral units of the crystal structure of $CoFe_{2-x}Ce_xO_4$ samples

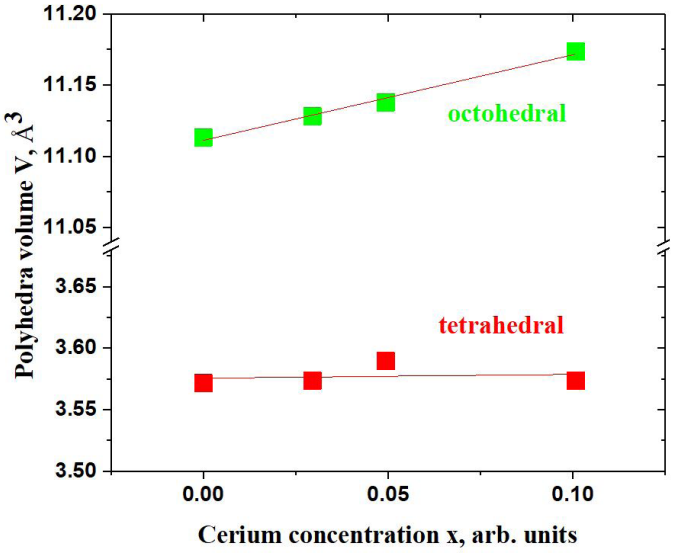

Figure 6: The volume of the octahedral B and tetrahedral A units of the crystal structure of $CoFe_{2-x}Ce_xO_4$ compounds as a function of cerium concentration. The experimental error does not exceed the size of the characters. The solid lines are linear approximation of experimental data

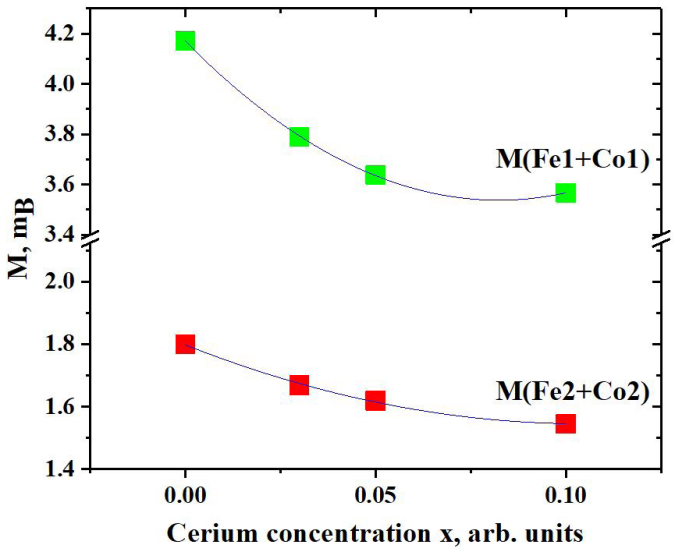

Figure 7: Dependence of the average magnetic moment on x for $CoFe_{2-x}Ce_xO_4$ ferrite. The experimental error does not exceed the size of the characters. The solid lines are polynomial linear approximation second order of experimental data

shown in Figure 6. The increase of the Fe/CoB-O bond length and the volume of the octahedra unit indicates the fact that cerium ions with a large ion radius embed in the octahedral units. It should be noted that the corresponding Fe/CoA-O bond length of tetragonal oxygen units and its volume does not change under the cerium doping. Under cerium increasing the bond angle Fe/CoA-O-Fe/CoB decrease from 123.5(4)° to 121.8(3)°.

It is known that the decrease in the valence angle means an increase in the structural disordering, which leads to a decrease in the magnetic moment of iron and cobalt in the appropriate crystallographic positions. The determined values of the average magnetic moments M_A and M_B of cobalt and iron magnetic ions in tetrahedral and octahedral crystallographic positions, respectively, were listed in Table 2. The magnetic moments M_A and M_B as a function of cerium concentration is presented in Figure 7. It is obvious that the increase of the cerium concentration leads to a decrease in the average magnetic moment not only in the octahedral position B where the cerium is embedded, but also in the tetragonal one. This is due to not only the change of weak magnetic interaction of J_{BB} but also changes in the dominant magnetic exchange J_{AB} [9, 10].

Conclusion

A mixture of pure $CoFe_2O_4$ and Co-ferrite doped Ce^{3+} ions have been prepared and studied in this study. The results of XRD confirm the formation of the samples in nano-scale with a single-phase cubic structure. VSM data shows that Ce^{3+} substitutes Fe^{3+} only in octahedral B-site, which indicates that the magnetic moment of B-site gradually reduces by further addition of Ce^{3+}. The disparity in ionic radii between Ce^{3+} and Fe^{3+} can causes a disturbance in the structure by producing strain and disorder in the electronic state. A closed hysteresis loops is obtained, which is a signature of the formation of a single domain and all the irreversible hysteresis processes are completed. The effect of Ce cerium concentration for $CoFe_{2-x}Ce_xO_4$ ferrite on their crystal and magnetic structure by neutron diffraction was investigated. The obtained values of the lengths of interatomic bonds and secondary of the magnetic moments in different crystallographic positions allow to identify structural mechanisms of formation of magnetic properties of ferrite $CoFe_{2-x}Ce_xO_4$ at different x.

References

1. R Valenzuela (2005) Magnetic ceramics. Cambridge University Press.

2. SS Ata-Allah, M Yehia, Physica B (2009) 404: 2382-8.

3. I Ya Korenblit, EF Shender (1984) Spin glasses. Knowledge M. 215C.

4. Belokon VI, Nefedev KV, Savunov MA (2006) Finite interaction range spin glass in the Ising model. Physics of the Solid State 48: 1746-53.

5. AL-HAJ Mansour (2005) Turk J Phys 29: 85-90.

6. B Cruz-Franco, T Gaudisson, S Ammar (2014) IEEE Transition on Magnetics 50: 4.

7. V Chlan (2010) Physics of Condensed Matter and Materials Research. F-3: 139.

8. Gorter EW (1954) Saturation magnetization and crystal chemistry of ferrimagnetic oxides. I. II. Theory of ferrimagnetism Philips Res Rep 9: 295-320.

9. VA Bokov (2002) Physics of magnetic materials: the textbook for high schools.

10. SM Yunus, HS Shim, CH Lee, MA Asgar, FU Ahmed, AKM Zakaria (2001) Neutron diffraction studies of the diluted spinel ferrite $Zn_xMg_{0.75-x}Cu_{0.25}Fe_2O_4$. Journal of magnetism and magnetic materials 232: 3.

11. Safontseva N, Yu, Nikiforov J (2001) On the Shape of Iron K Absorption Edges for Monoferrites with a Me(Mg, Mn, Ni, Zn)Fe_2O_4 Spinel Structure. Physics of the Solid State 43: 61-4.

12. EA Zhurakovsky, PP Kirichok (1985) Electronic States in ferrimagnets. Science's Dumka, Kiev.

13. Ferreira TAS, Waerenborgh JC, Mendonça MHRM, Nunes MR, Costa FM (2003) Structural and morphological characterization of $FeCo_2O_4$ and $CoFe_2O_4$ spinels prepared by a coprecipitation method. Solid State Sciences. 5: 383-92.

14. Wang, Zhongwu (2003) "High-pressure x-ray diffraction and Raman spectroscopic studies of the tetragonal spinel $CoFe_2O_4$." Physical Review B 68.9: 094101.

15. Argymbek BK, Kichanov SE, Kozlenko DP, Lukin EV, Morchenko AT, et al. (2018). Crystal and Magnetic Structures of Granular Powder Spinel Mn–Zn and Ni–Zn Ferrites. Physics of the Solid State, 60: 1727-32.

16. Kazin AP, Rumyantseva MN, Prusakov VE, Suzdalev IP, Gaskov AM (2012) Cation distribution in nanocrystalline $Ni_xZn_{1-x}Fe_2O_4$ spinel ferrites. Inorganic Materials, 48: 525-30.

17. Kozlenko DP, Belozerova NM, Ata-Allah SS, Kichanov SE, Yehia M, Hashhash A, et al. (2018) Neutron diffraction study of the pressure and temperature dependence of the crystal and magnetic structures of $Zn_{0.3}Cu_{0.7}Fe_{1.5}Ga_{0.5}O_4$ polycrystalline ferrite. J Magnet Magnetic Mat 449: 44-8.

18. Zakaria AKM, Asgar MA, Eriksson SG, Ahmed FU, Yunus SM, et al. (2003). The study of magnetic ordering in the spinel system $Zn_xNi_{1-x}FeCrO_4$ by neutron diffraction. J magnetism magnetic mat 265: 311-20.

19. Yunus SM, Azad AK, Eriksson SG, Eriksen J, Rundlöf H, et al. (2003) Studies of the magnetic behavior of the spinel system $Ga_xCoCrFe_{1-x}O_4$ by neutron diffraction. Physica B: Condensed Matter 337: 323-32.

20. Ata-Allah SS, Hashhash A (2006) Jahn–Teller effect and superparamagnetism in zn substituted copper-gallate ferrite. J magnetism magnetic mat 307: 191-7.

21. Ata-Allah SS (2004) Influence of Ga substitution on the magnetic and electric behavior of Cu0. 5Zn0. 5Fe2O4 compound. Journal of magnetism and magnetic materials, 284: 227-38.

22. A Hashhash, M Kisar (2016) influence of Ce-Substitution on Structural, Magnetic and Electrical Properties of Cobalt Ferrite Nanoparticles. J electronic mat 45: 462-72.

23. Kozlenko D, Kichanov S, Lukin E, Savenko B (2018) The DN-6 neutron diffractometer for high-pressure research at half a Megabar scale. Crystals 8: 331.

24. Rodríguez-Carvajal J (1993) Recent advances in magnetic structure determination by neutron powder diffraction. Physica B: Condensed Matter, 192: 55-69.

25. MA Almessiere, Y Slimani, M Sertkol, FA Khan, M Nawaz, et al. (2019) Ceramics International 45: 16147–16156
26. MA Almessiere, A Demir Korkmaz, Y Slimani, M Nawaz, S Ali, et al. (2019) Ceram Int 45: 3449–58.

27. Y Slimani, H Güngüneş, M Nawaz, A Manikandan, HS El Sayed, et al. (2018) Ceram Int 44: 14242–50.

28. MA Almessiere, Y Slimani, A Baykal (2018) Ceram Int 44: 9000.

29. Ghulam Mustafa, MU Islam, Wenli Zhang, Yasir Jamil, Abdul Waheed Anwar (2015) Mudassar Hussain, Mukhtar Ahmad, Journal of Alloys and Compounds 618: 428-36.

30. http://en.wikipedia.org/wiki/Cerium.

31. Y Koseoglu, A Baykal, F Gozuak, H Kavas (2009) Polyhedron 28: 2887–92.

32. Kh Roumaih (2011) J Mol Struct 1004: 1–7.

33. Gagan Dixit, Jitendra Pal Singh, RC Srivastava, HM Agrawal (2012) Journal of Magnetism and Magnetic Materials 324: 479–83.

34. V Verma, RK Kotnala,V Pandey, PC Kothari, L Radhapiyari, et al. (2008) J Alloys Compd 466: 404.

35. MA Almessiere, Y Slimani, AD Korkmaz, N Taskhandi, M Sertkol, et al. (2019) Ultrasonics - Sonochemistry 58: 104621.

36. A Nairan, M Khan, U Khan, M Iqbal, S. Riaz, et al. (2016) Nanomaterials 6: 73.

37. MA Almessiere, Y Slimani, S Guner, M Nawaz, A Baykal F, et al. (2019) Ceramics International 45: 8222-32.